
DAIR: DATA AUGMENTED INVARIANT REGULARIZATION

Tianjian Huang
University of Southern California
tianjian@usc.edu

Shaunak Halbe
College of Engineering Pune
halbasa18.comp@coep.ac.in

Chinnadhurai Sankar, Pooyan Amini, Satwik Kottur, Alborz Geramifard
Facebook AI
{chinnadhurai, pamini, skottur, alborzg}@fb.com

Meisam Razaviyayn
University of Southern California
razaviya@usc.edu

Ahmad Beirami
Facebook AI
beirami@fb.com

ABSTRACT

While deep learning through empirical risk minimization (ERM) has succeeded at achieving human-level performance at a variety of complex tasks, ERM generalizes poorly to distribution shift. This is partly explained by overfitting to spurious features such as background in images or named entities in natural language. Synthetic data augmentation followed by empirical risk minimization (DA-ERM) is a simple yet powerful solution to remedy this problem. In this paper, we propose data augmented invariant regularization (DAIR). The idea of DAIR is based on the observation that the model performance (loss) is desired to be consistent on the augmented sample and the original one. DAIR introduces a regularizer on DA-ERM to penalize such loss inconsistency. Both theoretically and through empirical experiments, we show that a particular form of the DAIR regularizer consistently performs well in a variety of settings. We apply it to multiple real-world learning problems involving domain shift, namely robust regression, visual question answering, robust deep neural network training, and task-oriented dialog modeling. Our experiments show that DAIR consistently outperforms ERM and DA-ERM with little marginal cost and setting new state-of-the-art results in several benchmarks.

1 Introduction

Deep neural networks are widely used in various applications ranging from computer vision to language processing. While deep learning has surpassed human-level performance in numerous tasks, neural networks are extremely vulnerable to overfitting to spurious correlations and therefore fail to generalize even under slight perturbations of the test distribution [Arjovsky et al., 2019]. This observation motivated the research community to tackle the problem of *domain generalization* (see [Ribeiro et al., 2020] for a detailed literature review). Recent benchmark datasets, such as Rotated MNIST [Arjovsky et al., 2019], Colored MNIST [Arjovsky et al., 2019], PACS [Li et al., 2017], VLCS [Fang et al., 2013], Office-Home [Venkateswara et al., 2017], Terra Incognita [Beery et al., 2018] and DomainNet [Peng et al., 2019], have shown difficulties for the generalization of deep neural network models under distribution shifts, and have sparked invention of many new algorithmic frameworks to address domain generalization.

A standard approach for improving out-of-distribution performance is to guarantee that learned representations are invariant to certain transformations. For example, image representations and trained models for computer vision should generally be invariant to rotations, changes in color, or background. There are two main directions for promoting such invariance to transformations, namely *data augmentation* and *geometric deep learning*.

Data augmentation promotes invariances in learned representations by curating synthetic examples that exhibit the desired invariances. Zhang et al. [2017] introduced mixup to train a neural network on convex combinations of pairs of

examples and their labels, which improves the generalization of state-of-the-art neural network architectures. Volpi et al. [2018] proposed an adaptive data augmentation method where adversarial examples are generated at every iteration, offering performance gain over unseen domains. Kuznichov et al. [2019] showed data augmentation can be applied to leaf segmentation by proposing a method that preserves the geometric structure of the data objects and keep the physical appearance of the data-set as close as possible to imaged plants in real agricultural scenes. The proposed method provides state of the art results when applied to the standard benchmark in the field. Tellez et al. [2019] showed stain color augmentation and stain color normalization could be used in computational pathology applications. Goel et al. [2020] proposed an approach to patch a model that fails due to spurious features on a real-world skin cancer dataset by data augmentation. Zhou et al. [2020] showed data augmentation with adversarial images could make the label classifier more robust to unknown domain shifts. Nam et al. [2021] improved domain generalization by reducing the intrinsic style bias of CNNs. This is achieved by training a separate network for randomizing the style of images and generating augmented data during training.

Geometric deep learning bakes such invariances into the neural network architecture. For example, convolutional layers [Lecun et al., 1998] are fundamentally preserving translations. There are other specifically designed networks to maintain invariances: Zaheer et al. [2017] studied the problem of designing models for machine learning tasks defined on sets and characterized the permutation invariant functions. Bloem-Reddy and Teh [2020] obtained generative functional representations of probability distributions that are invariant under the action of a compact group. Finzi et al. [2021] provided an algorithm for solving for the equivariant layers of matrix groups.

Besides two main directions mentioned above, researchers have proposed numerous algorithmic solutions to impose invariance and improve domain generalization: Ganin et al. [2016] introduced a new representation learning approach for domain adaptation, in which data at training and test time come from similar but different distributions. [Arjovsky et al., 2019] proposed invariant risk minimization (IRM) — a novel learning paradigm that estimates nonlinear, invariant, causal predictors from multiple training environments, to enable out-of-distribution generalization. The idea is to learn representations that perform equally well across different environments. Sagawa et al. [2019] introduced distributionally robust optimization (DRO) framework to learn models by minimizing the worst-case training loss over a set of pre-defined groups/environments. Li et al. [2018a] proposed a novel meta-learning method for domain generalization (MLDG), which simulates domain shift during training by synthesizing virtual testing domains within each mini-batch. Correlation alignment for deep domain adaptation [Sun and Saenko, 2016] (Deep CORAL) learns a nonlinear transformation that aligns correlations of layer activations in deep neural networks. Li et al. [2018b] extended adversarial autoencoders by imposing the Maximum Mean Discrepancy (MMD) measure to align the distributions among different domains, and matching the aligned distribution to a prior distribution via adversarial feature learning. Li et al. [2018c] proposed a conditional invariant neural network that minimizes the discrepancy in conditional distribution of images given the class labels across different domains. The approaches listed above are more complex than simple training mechanisms such as empirical risk minimization (ERM) and hence they cannot be easily applied to involved tasks such as training generative models. In contrast, Gulrajani and Lopez-Paz [2020] demonstrated that the simple ERM method can achieve state of the art performance after fine-tuning in various datasets/applications. However, there are still problem instances that ERM performs very poorly. For example, in learning end-to-end dialogue models, Qian et al. [2021] showed 29% performance drop on MultiWOZ [Budzianowski et al., 2018] due to the memorization of named entities.

In this paper, we propose a regularization technique, called data augmented invariant regularization (DAIR) that penalizes the inconsistency of loss on augmented samples with respect to the original ones. DAIR is applicable whenever data augmentation is used to promote invariances. DAIR only requires marginal additional cost on top of data augmentation, and is simple and applicable to a wide host of supervised and unsupervised learning tasks, including generative models. We introduce the DAIR formulation, motivate it, and theoretically prove some of its properties in Section 2. We empirically evaluate DAIR on a variety of problem setups ranging from defense against adversarial attacks to domain generalization in the presence of environment shift in Section 3. Our experimental results show that DAIR is competitive with or even outperforms state-of-the-art algorithms specifically designed for imposing invariance in these problems.

2 DAIR: Data Augmented Invariant Regularization

For a data sample $z = (x, y)$, let $\ell(z; \theta)$ be its parametric loss function, where θ is the set of model parameters (e.g., network weights). The popular Empirical Risk Minimization (ERM) framework trains the model by minimizing the expected value of the following loss over the training data:

$$f_{\text{ERM}}(z; \theta) = \ell(z; \theta). \tag{ERM}$$

We assume that we have access to a (potentially randomized) data augmenter function $A(\cdot)$. Examples for A include (random) rotation, change of background, or change of entity names. Such augmenters aim at capturing the transformations against which we wish to be invariant to. Given a sample z , let $\tilde{z} = (\tilde{x}, \tilde{y}) = A(z)$ denote an augmented sample. Previous work has used both original and augmented examples during training, which leads to the following standard objective function, called Data Augmented Empirical Risk Minimization (DA-ERM):

$$f_{\text{DA-ERM}}(z, \tilde{z}; \theta) = \frac{1}{2}\ell(z; \theta) + \frac{1}{2}\ell(\tilde{z}; \theta). \quad (\text{DA-ERM})$$

While DA-ERM has been successful in many applications, one natural question is whether we can further improve over it using the knowledge that the performance on augmented samples should be consistent with the original ones. We propose the data augmented invariant regularization (DAIR) framework, which further penalizes DA-ERM for any such inconsistency. With DAIR, the objective function becomes

$$\begin{aligned} f_{\text{DAIR}, \mathcal{R}, \lambda}(z, \tilde{z}; \theta) &= f_{\text{DA-ERM}}(z, \tilde{z}; \theta) + \lambda \mathcal{R}(z, \tilde{z}; \theta) \\ &= \frac{1}{2}\ell(z; \theta) + \frac{1}{2}\ell(\tilde{z}; \theta) + \lambda \mathcal{R}(z, \tilde{z}; \theta), \end{aligned} \quad (\text{DAIR})$$

where the goal of the regularizer is to maintain the performance of the model on z and \tilde{z} similar. Similar augmentation ideas have been utilized in the past for special standard regularizers in limited applications such as training adversarially robust neural networks [Engstrom et al., 2018, Kannan et al., 2018, Zhang et al., 2019]. In this work, we show that with proper form of regularization, this simple approach is indeed competitive to the state-of-the-art methods for imposing invariance. To proceed, consider a supervised learning task and let $\mathbf{q}(z; \theta)$ be the output of the model right after the softmax layer. If we treat the loss function as (un-normalized) negative log-likelihood of the output distribution, and let $\mathbf{q}(z; \theta) \propto e^{-\ell(z; \theta)}$, then we can consider $\mathcal{R}(\cdot)$ to be any proper divergence between the output distributions $\mathbf{q}(z; \theta)$ and $\mathbf{q}(\tilde{z}; \theta)$, such as \mathcal{L}_2 distance or KL divergence, which will promote $\mathbf{q}(z; \theta) \approx \mathbf{q}(\tilde{z}; \theta)$. As it turns out in the rest of this section, we are particularly interested in the following particular form of the regularizer:

$$\mathcal{R}_{\text{sq}}(z, \tilde{z}; \theta) := \left(\sqrt{\ell(z; \theta)} - \sqrt{\ell(\tilde{z}; \theta)} \right)^2, \quad (\text{SQ Regularizer})$$

and we call this variant DAIR-SQ. The idea behind DAIR-SQ is to simply promote $\ell(z; \theta) \approx \ell(\tilde{z}; \theta)$, and ignore the rest of the possible outcomes of y . Further justification on this special type of regularizer will be provided through the rest of this section.

2.1 What does DAIR offer beyond DA-ERM?

To motivate the introduction of the DAIR regularizer, we first consider a simple setup through which we demonstrate that DAIR fundamentally outperforms DA-ERM. Consider a linear regression problem where at the training time the input is $\mathbf{x}_{\text{train}} = (x, s = y)$ and the label y , i.e., $z_{\text{train}} = (\mathbf{x}_{\text{train}}, y)$. Here, $x \sim \mathcal{N}(0, \sigma_x^2)$, and $y = x + \varepsilon$, where ε is independent of x and $\varepsilon \sim \mathcal{N}(0, \sigma_\varepsilon^2)$. In this example, the target is explicitly provided as a spurious feature to the learner at the training time. At test time, the spurious feature is absent, i.e., $\mathbf{x}_{\text{test}} = (x, s = 0)$.

Clearly, in this toy example, the optimal regressor is $w^* = (w_1^*, w_2^*)^\top = (1, 0)^\top$. However, absent the knowledge of the spurious feature vanilla ERM will learn $w_{\text{ERM}} \approx (0, 1)^\top$, completely overfitting the spurious feature. We assume that the learner has access to a data augmentation module that generates $\tilde{z} = A(z; a, \sigma_n^2) = (\mathbf{x}_{\text{aug}}, y)$, such that $\mathbf{x}_{\text{aug}} = (x, s = ay + n)$ where $n \sim \mathcal{N}(0, \sigma_n^2)$. The augmented data will encourage the learned model to become invariant to the spurious feature. In Figure 1, we perform simulations with $a = 0.5$, $\sigma_x^2 = 1$, $\sigma_\varepsilon^2 = 0.25$, $\sigma_n^2 = 0.1$ and plot four lines associated with each regressor with the slope of their respective w_1 . We ignore w_2 as the second spurious feature is absent at test time and hence w_2 does not impact test performance. The optimal regressor is shown as the blue line, with a slope of 1. ERM (red line) completely fails due to the overfitting to the spurious feature. DA-ERM (orange line) significantly improves over ERM but still is far from optimal performance. DAIR-SQ (purple line) almost recovers the optimal solution. This is not a coincidence. We prove that DAIR-SQ is optimal for a class of linear regression problems, while DA-ERM does not approach optimal performance even in the limit of infinite samples.

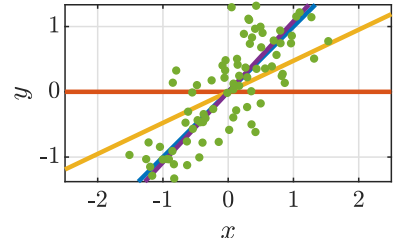


Figure 1: The plot of the optimal, ERM, DA-ERM and DAIR-SQ regressor, where $a = 0.5$, $\sigma_x^2 = 1$, $\sigma_\varepsilon^2 = 0.25$, $\sigma_n^2 = 0.1$.

Proposition 1. Consider the class of linear regression problems described above with a spurious feature (highly correlated with the output). Assume that the learner has access to a data augmentation module that perturbs the

spurious feature. Then, for any value of a and σ_n , DAIR-SQ achieves optimal test error as number of samples grows and $\lambda \rightarrow \infty$. On the other hand, DA-ERM cannot recover optimal performance even in the limit of infinite training data unless $\sigma_n \rightarrow \infty$.

Rigorous statement and proof of Proposition 1 is relegated to Appendix A. While we only analyzed DAIR-SQ, we believe the content of this proposition should extend to other variants of DAIR as well.

Note that when $\sigma_n \rightarrow \infty$, DA-ERM could also recover w^* . One can interpret that when $\sigma_n \rightarrow \infty$, the augmenter is so strong forcing w_2 to vanish. It worth nothing that DAIR could recover w^* with a much weaker augmenter. This is crucial since in real-world applications, strong augmented examples typically require to be carefully designed and are not always available. We will expand on this in Section 2.2.

2.2 Which variant of DAIR should we use?

In this section, we empirically compare ERM, DA-ERM and different variants of DAIR to choose a DAIR variant for subsequent real-world experiments.

Rotated MNIST [Ghifary et al., 2015] is a dataset where MNIST digits are rotated. We work with two different sets of degrees of rotation for Rotated MNIST. The first one is *Weak Rotation* where the digits are rotated uniformly at random $[0, \frac{\pi}{6})$ radians. In *Strong Rotation* the digits are rotated uniformly at random $[0, 2\pi)$ radians. To evaluate the robustness of the methods, we further add label noise at training time where the label is replaced with a digit chosen from $\{0, \dots, 9\}$ uniformly at random with a certain probability. No label noise is added at test time. Detailed setup can be found in Appendix D.

In the first experiment, we use Weak Rotation for data augmentation while at test time we use Strong Rotation. Thus, some test time rotations have not been observed at training time. Figure 2 shows the test performance of all algorithms (averaged over three runs) as a function of λ . As can be seen, ERM (with no data augmentation) does not generalize to rotated test images and performs poorly. DA-ERM offers significant performance improvement over ERM. When λ is very small all variants of DAIR are virtually the same as DA-ERM, too. DAIR-SQ and KL regularizer outperform other regularizers and are the only two variants that offer improvement over DA-ERM. The other DAIR variants did not offer improvement over DA-ERM and converged to poor local minima with 10% test accuracy (random) for large λ . We were not able to remedy this by tuning of their step size. As the label noise level becomes larger, DAIR-SQ is more robust than KL and offers the best performance.

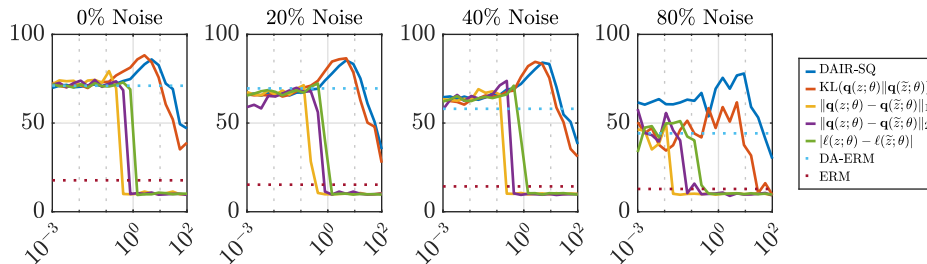


Figure 2: Test accuracy as a function of λ for different noise levels for **Weak Rotation** augmentation.

The setup for the second experiment is the same as the first one, except we also use Strong Rotation in training for augmentation, so there is no distribution shift for DA-ERM. As can be seen in Figure 3, data augmentation achieves very good performance in this case and none of the DAIR regularizers offer any improvement beyond data augmentation. We suspect this to be true in general; if the data augmentation is well-devised and optimized the resulting model could become invariant to the desired transformations at test time. This observation agrees with the toy example in Section 2.1. Under the scenario of strong augmentation, i.e. $\sigma_n^2 \rightarrow \infty$, DA-ERM could behave similarly as DAIR. However, in practice, we often are to cope with some degree of distribution shift at test time.

Colored MNIST [Arjovsky et al., 2019] is a binary classification task built on the MNSIT dataset. Digits 0-4 are labeled 1; whereas digits 5-9 are labeled 0. Additionally, 25% label noise is added, i.e., the labels are flipped with probability 0.25, both at train and test time, capping the achievable test accuracy to 75%. In this dataset, each digit is RGB colored. During training, label 1 is given the color green with probability 0.9 and red with probability 0.1. On the other hand, label 0 is given red color with probability 0.9 and green with probability 0.1. This introduces a high degree of spurious correlation between color and the label. Thus, ERM is expected to significantly overfit to color for predicting the label.

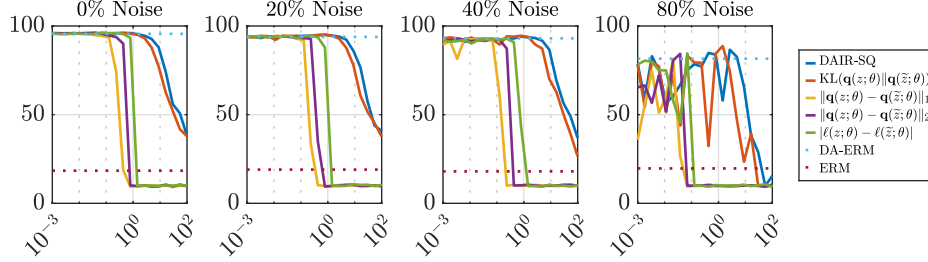


Figure 3: Test accuracy as a function of λ for different noise levels for **Strong Rotation** augmentation.

At test time, the correlation with color is reversed for digits. Hence, vanilla ERM is expected to perform worse than 50% coin flip at test time. We explore two data augmentation schemes in this experiment. For the *Adversarial Augmentation* (*Adv. Aug.*) setup, the augmented images will have their color flipped (from red to green or vice versa) with probability 0.1. For the *Random Augmentation* (*Rnd. Aug.*) setup, the augmented images are colored uniformly at random. Detailed description of the setup can be found in Appendix D.

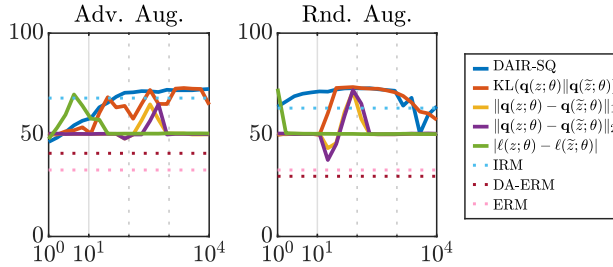


Figure 4: Test accuracy vs λ on Colored MNIST for Adversarial Color augmentation and Random Color augmentation.

Figure 4 suggests that DAIR-SQ and KL achieve $\sim 72\%$ test accuracy using both augmentation schemes, outperforming the state-of-the-art 68% test accuracy reported by invariant risk minimization (IRM) [Arjovsky et al., 2019], and almost reaching the 75% cap. We note however that this comparison may be unfair because IRM does not have access to any augmented samples, which leak information about the environment. We also notice that neither variant of DA-ERM achieves test performance better than 50% coin flip in this experiment, while DA-ERM with Adversarial Augmentation performs better compared to Random Augmentation. Comparing different regularizers, we conclude that DAIR-SQ is more stable and robust than other regularizers followed by KL.

2.3 Further justification for DAIR-SQ

The regularization function in Eq. (SQ Regularizer) is designed to ensure that $\mathcal{R}_{\text{sq}}(\cdot)$ and $\ell(\cdot)$ scale proportionally, making it easier to tune λ across different tasks. While we have already compared DAIR-SQ with several alternatives, we want to specifically focus on a closely related one, i.e., $\mathcal{R}_1(z, \tilde{z}; \theta) = |\ell(z; \theta) - \ell(\tilde{z}; \theta)|$ (DAIR-L1). Compared with KL divergence regularization, both DAIR-L1 and DAIR-SQ enjoy the simplicity and computational efficiency, especially when the cardinality of the output is large, e.g., language models where output vector dimension is the same as the vocabulary size. As opposed to KL, they are also directly applicable to regression with uncountable output. However, as we already observed in Section 2.2, DAIR-L1 either outright failed or was unstable on majority of the experiments we have performed so far. The following lemma further investigates the discrepancy between DAIR-SQ and DAIR-L1:

Lemma 1. For any non-negative loss function ℓ ,

$$\mathcal{R}_1(z, \tilde{z}; \theta) - \mathcal{R}_{\text{sq}}(z, \tilde{z}; \theta) = 2\sqrt{\min\{\ell(z; \theta), \ell(\tilde{z}; \theta)\}\mathcal{R}_{\text{sq}}(z, \tilde{z}; \theta)} \geq 0.$$

Thus, $\mathcal{R}_1(z, \tilde{z}; \theta) \geq \mathcal{R}_{\text{sq}}(z, \tilde{z}; \theta)$ with equality if and only if $\ell(\tilde{z}; \theta) = 0$ or $\ell(z; \theta) = 0$ or $\ell(\tilde{z}; \theta) = \ell(z; \theta)$.

The proof of Lemma 1 appears in Appendix A. The difference is depicted in Figure 5. This suggests that $\mathcal{R}_{\text{sq}}(z, \tilde{z}; \theta)$ incurs a much smaller penalty when $\ell(z; \theta)$ is large. On the other hand, when $\ell(z; \theta) \approx 0$ the regularizer is much stronger and almost equivalent to \mathcal{R}_1 . Why does this matter? At the beginning of training when the network is not yet

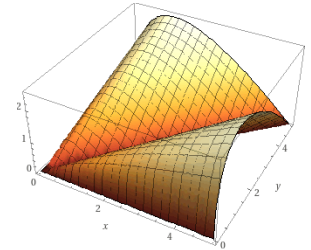


Figure 5: The plot of $\mathcal{R}_1(z, \tilde{z}; \theta) - \mathcal{R}_{\text{sq}}(z, \tilde{z}; \theta)$.

trained, the loss values on the original samples are large, and the \mathcal{R}_{sq} regularizer is weak letting the training to proceed towards a good solution for the original samples. As the network is being trained on original samples and their loss is vanishing, the regularizer starts to force the network to become invariant on the augmented samples. We suspect this to be the reason that DAIR-SQ outperforms DAIR-L1, which was unstable and converged to bad local minima.

This same property of DAIR-SQ regularizer also weakens the regularizer on training samples with high losses at the later stages of training. These samples are likely noisy, which makes DAIR-SQ more robust to noisy samples, as we already observed in Section 2.2.

2.4 The impact of partial augmentation

We explore the impact of partial augmentation, where we only augment a certain fraction of the training samples. The experiment revisits noiseless Rotated MNIST with weak rotation data augmentation and Colored MNIST with Adversarial augmentation. This experiment emulates situations where an augmentation function is only applicable to certain examples or where augmentation is expensive and we would like to decrease the augmentation cost. In Figure 6, we report the experiment results for DA-ERM and DAIR-SQ by applying augmentation only {10%, 20%, 30%, 50%, 100%} of the training samples, averaged on three runs. In Rotated MNIST experiment, as can be seen, DAIR-SQ with augmentation on only 20-30% of the samples performs similar to full augmentation. On the other hand, DA-ERM is more sensitive to partial augmentation and is subject to a steeper performance drop. This could be viewed as further evidence that DAIR-SQ could reach its best performance using weak augmenter functions. It is also noteworthy that in this example, DAIR-SQ with only 10% partial augmentation still outperforms DA-ERM with 100% augmentation. One can draw similar conclusion in the Colored MNIST experiment as only 10% augmentation gives comparable performance to full augmentation.

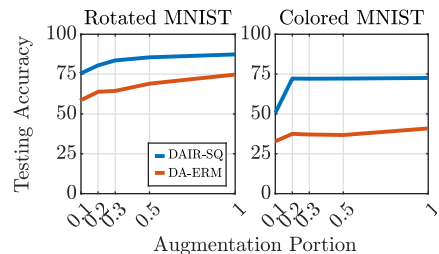


Figure 6: Test accuracy vs fraction of augmented samples on Rotated MNIST.

3 Experiments

In this section, we apply DAIR to some real-world tasks and compare its performance with state-of-the-art baselines for these tasks.

3.1 Robust Regression: Simultaneous domain shift and label noise

In this experiment, we consider a regression task to minimize the root mean square error (RMSE) of the predicted values on samples from the Drug Discovery dataset. The task is to predict the bioactivities given a set of chemical compounds (binary features). We follow the setup of Li et al. [2021] to introduce random noise to corrupt the targets. Furthermore, similar to Colored MNIST, we add a spurious binary feature to the original setup. At training time, the spurious feature is set to 1 if a particular target is above the median of the all the targets in the training samples, and 0 otherwise. At test time, this condition is reversed leading to poor generalization. We compare using ERM, DA-ERM and DAIR-SQ formulations under 0%, 20% and 40% noise levels on three baselines: \mathcal{L}_2 loss, Huber loss, and negatively tilted loss [Li et al., 2021], which is called tilted empirical risk minimization (TERM) and is designed for robust regression. For each of these baselines, we perform data augmentation by randomly assigning the spurious feature as 0 or 1 with equal probability. Finally, we apply the DAIR-SQ regularizer to each of these loss functions.

Table 1: Test RMSE (with standard error) for varying degrees of label noise for ERM, DA-ERM, and DAIR using different losses.

Algorithms	Test RMSE (Drug Discovery dataset)									
	0% Noise			20% Noise			40% Noise			Clean
	-	DA-	DAIR	-	DA-	DAIR	-	DA-	DAIR	-
\mathcal{L}_2 loss	1.97 (0.00)	1.36 (0.00)	1.23 (0.00)	4.33 (0.04)	2.52 (0.05)	2.04 (0.06)	5.30 (0.04)	3.47 (0.07)	2.99 (0.09)	1.23 (0.00)
Huber [Huber, 1964]	1.84 (0.00)	1.27 (0.00)	1.24 (0.00)	2.93 (0.05)	1.50 (0.02)	1.39 (0.02)	4.40 (0.07)	2.18 (0.04)	1.70 (0.05)	1.16 (0.00)
TERM [Li et al., 2021]	1.74 (0.00)	1.26 (0.00)	1.25 (0.00)	1.87 (0.01)	1.27 (0.01)	1.27 (0.01)	2.01 (0.02)	1.33 (0.01)	1.31 (0.01)	1.23 (0.00)

The results of this experiment are reported in Table 1. In the last column of the table we report results on the clean dataset without any spurious features for comparison purposes. As can be seen, without data augmentation all methods

fall prey to spurious features and perform poorly, especially as the noise level is increased. It is noteworthy that while TERM is not designed for domain shift, it slightly outperforms the other baselines in the presence of spurious features showing that TERM has some inherent robustness to the domain shift. By adopting data augmentation, testing error decreases but is still quite large as compared to the Clean ERM setup for high values of noise. Notably, DAIR is able to reduce the testing error across all objectives and noise levels with the gap between DAIR and other approaches increasing with the degree of noise. For the 0% noise setup, DAIR is able to almost recover the Clean ERM accuracy for all three objectives. The gains achieved with DAIR are prominent for \mathcal{L}_2 and Huber, but marginal for TERM. Finally, data augmentation/DAIR combined with TERM can simultaneously handle domain shift and noisy labels as can be seen in this table.

3.2 Visual Question Answering

Visual Question Answering (VQA) has diverse applications ranging from visual chatbots to assistants for the visually impaired. In such real-world settings, it is desirable for VQA models to be robust to variations in the input modalities. In this spirit, recent works [Agarwal et al., 2020, Shah et al., 2019, Ray et al., 2019] have studied the robustness and consistency of VQA models under linguistic and visual variations. In this paper, we focus on the InVariant VQA (IV-VQA) dataset which contains semantically edited images corresponding to a subset of the original images from VQA v2 [Goyal et al., 2017]. For each image in this subset, IV-VQA contains one or more edited images constructed by removing an object which is irrelevant to answering the question. A robust model should be invariant to such edits by making the same predictions on the edited image.

We choose the attention based SAAA [Kazemi and Elqursh, 2017] model to match the original setup from Agarwal et al. [2020]. All the approaches from Table 2 use the original VQA v2 ‘train’ split for training, along with the IV-VQA ‘train’ split for augmentation in the DAIR and DA-ERM settings. The ERM setup, represents a vanilla SAAA model trained on the VQA v2 ‘train’ split. For the data augmentation methods, if an image from VQA v2 contains its corresponding edited versions in IV-VQA, we randomly select one of them to serve as an augmentation during training. Using DAIR, we enforce consistency in predictions between the original and edited samples. Wherever, the edited image is not available, the DAIR formulation reduces to ERM. We use the standard VQA accuracy along with the consistency metrics proposed in Agarwal et al. [2020] to compare our results against the ERM setup and the DA-ERM approach discussed in Agarwal et al. [2020]. These baseline models are trained and evaluated by us, using the same training setup as DAIR.

Algorithm	ERM (%) [Kazemi and Elqursh, 2017]	DA-ERM (%) [Agarwal et al., 2020]	DAIR-SQ (%)
VQA v2 val	57.10	57.30	57.54
Predictions flipped	11.84	11.68	10.37
pos → neg	4.58	4.40	3.80
neg → pos	5.17	5.14	4.65
neg → neg	2.08	2.14	1.91

Table 2: Accuracy and Consistency metrics on VQA v2 val & IV-VQA test set.

The results are reported in Table 2. We measure the accuracy on the original VQA v2 ‘val’ set and the consistency metrics across edited IV-VQA instances and their corresponding real instances from VQA v2 ‘val’ set. The accuracy of DAIR on the VQA v2 validation set is still higher as compared to others, while improving over all baselines by a minimum of **1.31%** under the ‘Predictions flipped’ metric which is the sum of the three types of flips (pos → neg, neg → pos and neg → neg). This improvement is significant given that the model needs to predict the answer correctly from 3000 candidate answers. While applying DAIR to this task, we observe a trade-off between the VQA accuracy on ‘val’ and the ‘Predictions flipped’ percentage controlled by the λ parameter. By increasing λ , the ‘Predictions flipped’ percentage decreases, and drops to as low as 7-8% when λ is at 10, albeit sacrificing the VQA accuracy by 5-6%. Thus, for moderate values of λ , DAIR is able to maintain the predictive power while enforcing consistency across variations in the visual space.

3.3 Training Robust Deep Networks

Deep neural networks have been widely used in various applications, especially in the field of image recognition. However, these networks are vulnerable to adversarial attacks that use small imperceptible perturbations in the input data to significantly change the network’s output. In this section, we demonstrate that our regularizer can be applied to

#	Algorithm	Clean (%)	FGSM (%)	PGD20 (%)
1	PGD Training [Madry et al., 2018]	82.89	55.38	48.40
2	APART [Li et al., 2020]	82.45	55.33	48.95
3	DAIR-SQ ($\lambda = 6$)	83.04	57.57	50.68
4	TRADES + ATTA [Zheng et al., 2020]	78.98	55.58	52.30
5	TRADES [Zhang et al., 2019]	81.67	57.78	52.90
6	DAIR-SQ ($\lambda = 16.7$)	81.29	58.58	53.37

Table 3: CIFAR-10 test accuracies under FGSM and PGD attacks.

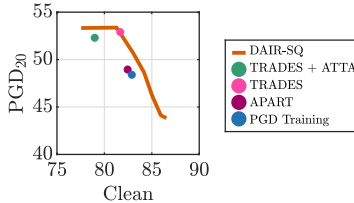


Figure 7: Trade-off between accuracies under clean and adversarial setup by tuning λ

train robust neural networks and it achieves comparable or better results than baseline models from state-of-the-art approaches which are specifically designed for this task. In our approach, the augmented examples \tilde{z} can be generated by a certain strong attack, such as Projected Gradient Descent (PGD) [Madry et al., 2018] or CW [Carlini and Wagner, 2017]. We argue that our approach achieves results competitive with the state-of-the-art, is extremely simple to implement and adds a negligible computation cost.

We conduct our experiments on CIFAR-10 dataset. For all algorithms from Table 3, we utilize a Pre-Activation ResNet-18 [He et al., 2016] for classification, with a last-layer output size of 10. For training the DAIR based model, the adversarial examples are generated by l_∞ based PGD attack with 11 iterations, ϵ set to $8/255$ and attack step size to $2/255$. We apply DAIR with λ set to 16 and run 120 epochs on the training datasets. We evaluate all the models against the Fast Gradient Sign Method [Goodfellow et al., 2015] (FGSM) attack and PGD with 20 iterations for the same perturbation sizes.

We compare our approach with several approaches among which TRADES [Zhang et al., 2019] is the state of the art for robust accuracy on CIFAR-10. The performance of our algorithm against FGSM and variants of PGD, is summarized in Table 3, which shows that our results are competitive with the state-of-the-art algorithms. We report the performance of DAIR-SQ in Table 3 based on the configurations that give the best Clean accuracy (row 3) and the best Robust accuracy against PGD20 (row 6). The trade-off curve shown in Figure 7 suggests that by sweeping the value of λ , DAIR-SQ can achieve a better clean accuracy but a slightly lower PGD20 accuracy, and dominates most of the baseline, while it achieves a similar performance with TRADES. Note that the formulation in TRADES is equivalent to DAIR with a KL divergence regularizer between the logits of the original and adversarial images. As opposed to our setup, the regularizer term in TRADES is also used in solving the maximization problem to generate adversarial images.

3.4 Task-Oriented Dialog

Virtual digital assistants (e.g., Amazon Alexa, Apple Siri and Facebook Portal) that engage in conversations with human users are rapidly gaining popularity. These devices require the modelling of task-oriented dialog systems that can communicate with users through natural language to accomplish a wide range of tasks. Among task-oriented dialog datasets, MultiWOZ [Budzianowski et al., 2018] has gained the most popularity owing to the availability of 10k+ realistic dialogs across 8 different domains, and has been improved several times [Wu et al., 2019, Eric et al., 2019, Zang et al., 2020, Han et al., 2021, Qian et al., 2021].

Recently, SimpleTOD [Hosseini-Asl et al., 2020] achieved state-of-the-art results on MultiWOZ using a neural end-to-end modeling approach. However, it was observed in [Qian et al., 2021] that the performance of SimpleTOD drops significantly when the test set named entities are replaced with new ones never observed during training, perhaps due to the memorization of named entities. As a new benchmark, Qian et al. [2021] proposed a new test set for MultiWOZ 2.2, called MultiWOZ 2.2 with SGD entities, where named entities are replaced with those from Schema Guided Dialog dataset [Rastogi et al., 2020] and showed that SimpleTOD [Hosseini-Asl et al., 2020] endures more than 8% performance drop on the new test set. In this section, we leverage DAIR-SQ to promote invariance of the dialog policy to named entities in the dialog flow. To this end, we measure the performance both on MultiWOZ 2.2 [Zang et al., 2020] and MultiWOZ 2.2 with SGD entities [Qian et al., 2021].

To address this problem, we define a new data augmentation scheme for DAIR and DA-ERM by replacing the named entities from the MultiWOZ 2.2 training set with randomly scrambled versions of the named entities. For example, “cambridge” could be turned into “gacrimebd”. In all of our experiments, we utilize the SimpleTOD model [Hosseini-Asl et al., 2020] which is the state-of-the-art for Dialog State Tracking (DST), and we apply DAIR to enforce invariance between the named entities in the training examples and the scrambled entities from their corresponding augmented samples.

The results are presented in Table 4, where performance is measured in Joint Goal Accuracy (JGA). JGA is a binary metric, and is equal to 1 if the predictions of all slot values in a turn are correct. As can be seen, both DA-ERM

Test set	SimpleTOD [Hosseini-Asl et al., 2020]	SimpleTOD (DA-)	SimpleTOD (DAIR)
MultiWOZ 2.2 [Zang et al., 2020]	0.5483	0.5915 _(0.0055)	0.5998 _(0.0030)
MultiWOZ 2.2 w/ SGD entities [Qian et al., 2021]	0.4844	0.5311 _(0.0074)	0.5609 _(0.0074)

Table 4: Joint Goal Accuracy (JGA) for different approaches on the SimpleTOD model. DAIR achieves SOTA on the original and well as the new test set.

and DAIR outperform SimpleTOD [Hosseini-Asl et al., 2020] on MultiWOZ 2.2 w/ SGD entities. Perhaps, more surprisingly, they also outperform SimpleTOD on the original MultiWOZ 2.2 test set with no distribution shift, which we attribute to better robustness to named entity memorization. This leads to DAIR-SQ setting new state-of-the-art results on both benchmarks.

4 Conclusion

In this paper, we proposed a simple yet effective regularizer that can be used wherever data augmentation is used to promote invariance. We rigorously showed that our proposed regularizer can recover the optimal solution in certain regression task where simple data augmentation can not. We also compare our DAIR-SQ regularizer with the existing off-the-shelf regularizers such as \mathcal{L}_1 , \mathcal{L}_2 and KL divergence. We empirically showed that the DAIR-SQ regularizer is competitive with or outperforms state-of-the-art problem-specific baselines in a variety of problem setups. We evaluated DAIR in four different categories of machine learning tasks including regression, visual question answering, and training robust deep neural networks, and task-oriented dialog modeling. This is a major benefit of DAIR-SQ as some of other regularizers cannot be applied to regression tasks. Empirically the proposed algorithm outperforms well in all tasks. Better understanding of the tuning of the corresponding hyperparameter also remains as an open area for research. Finally, a more in-depth theoretical understanding of the properties of DAIR-SQ regularizer that lead to its superior empirical performance are also important questions for future work. While we showed that DAIR-SQ boosts existing performance metrics, such as average accuracy, the interplay of DAIR-SQ with other metrics, especially group fairness is also another important area for future research.

References

- V. Agarwal, R. Shetty, and M. Fritz. Towards causal VQA: Revealing and reducing spurious correlations by invariant and covariant semantic editing. In *Proceedings of the IEEE Conference on Computer Vision and Pattern Recognition*, 2020.
- M. Arjovsky, L. Bottou, I. Gulrajani, and D. Lopez-Paz. Invariant risk minimization. *arXiv preprint arXiv:1907.02893*, 2019.
- S. Beery, G. Van Horn, and P. Perona. Recognition in terra incognita. In *Proceedings of the European Conference on Computer Vision (ECCV)*, pages 456–473, 2018.
- B. Bloem-Reddy and Y. W. Teh. Probabilistic symmetries and invariant neural networks. *J. Mach. Learn. Res.*, 21: 90–1, 2020.
- P. Budzianowski, T.-H. Wen, B.-H. Tseng, I. Casanueva, S. Ultes, O. Ramadan, and M. Gašić. Multiwoz—a large-scale multi-domain wizard-of-oz dataset for task-oriented dialogue modelling. *arXiv preprint arXiv:1810.00278*, 2018.
- N. Carlini and D. Wagner. Towards evaluating the robustness of neural networks, 2017.
- L. Engstrom, A. Ilyas, and A. Athalye. Evaluating and understanding the robustness of adversarial logit pairing. *arXiv preprint arXiv:1807.10272*, 2018.
- M. Eric, R. Goel, S. Paul, A. Sethi, S. Agarwal, S. Gao, and D. Hakkani-Tur. Multiwoz 2.1: Multi-domain dialogue state corrections and state tracking baselines. *arXiv preprint arXiv:1907.01669*, 2019.
- C. Fang, Y. Xu, and D. N. Rockmore. Unbiased metric learning: On the utilization of multiple datasets and web images for softening bias. In *Proceedings of the IEEE International Conference on Computer Vision*, pages 1657–1664, 2013.
- M. Finzi, M. Welling, and A. G. Wilson. A practical method for constructing equivariant multilayer perceptrons for arbitrary matrix groups. *arXiv preprint arXiv:2104.09459*, 2021.

- Y. Ganin, E. Ustinova, H. Ajakan, P. Germain, H. Larochelle, F. Laviolette, M. Marchand, and V. Lempitsky. Domain-adversarial training of neural networks. *The journal of machine learning research*, 17(1):2096–2030, 2016.
- M. Ghifary, W. B. Kleijn, M. Zhang, and D. Balduzzi. Domain generalization for object recognition with multi-task autoencoders. In *Proceedings of the IEEE international conference on computer vision*, pages 2551–2559, 2015.
- K. Goel, A. Gu, Y. Li, and C. Ré. Model patching: Closing the subgroup performance gap with data augmentation. *arXiv preprint arXiv:2008.06775*, 2020.
- I. J. Goodfellow, J. Shlens, and C. Szegedy. Explaining and harnessing adversarial examples, 2015.
- Y. Goyal, T. Khot, D. Summers-Stay, D. Batra, and D. Parikh. Making the V in VQA matter: Elevating the role of image understanding in Visual Question Answering. In *Conference on Computer Vision and Pattern Recognition (CVPR)*, 2017.
- I. Gulrajani and D. Lopez-Paz. In search of lost domain generalization. *arXiv preprint arXiv:2007.01434*, 2020.
- T. Han, X. Liu, R. Takanobu, Y. Lian, C. Huang, D. Wan, W. Peng, and M. Huang. Multiwoz 2.3: A multi-domain task-oriented dialogue dataset enhanced with annotation corrections and co-reference annotation, 2021.
- K. He, X. Zhang, S. Ren, and J. Sun. Identity mappings in deep residual networks, 2016.
- E. Hosseini-Asl, B. McCann, C.-S. Wu, S. Yavuz, and R. Socher. A simple language model for task-oriented dialogue, 2020.
- P. J. Huber. Robust estimation of a location parameter. *Annals of Mathematical Statistics*, 35:492–518, 1964.
- H. Kannan, A. Kurakin, and I. Goodfellow. Adversarial logit pairing. *arXiv preprint arXiv:1803.06373*, 2018.
- V. Kazemi and A. Elqursh. Show, ask, attend, and answer: A strong baseline for visual question answering. *ArXiv*, abs/1704.03162, 2017.
- D. Kuznichov, A. Zvirin, Y. Honen, and R. Kimmel. Data augmentation for leaf segmentation and counting tasks in rosette plants. In *Proceedings of the IEEE/CVF Conference on Computer Vision and Pattern Recognition Workshops*, pages 0–0, 2019.
- Y. Lecun, L. Bottou, Y. Bengio, and P. Haffner. Gradient-based learning applied to document recognition. *Proceedings of the IEEE*, 86(11):2278–2324, 1998. doi: 10.1109/5.726791.
- D. Li, Y. Yang, Y.-Z. Song, and T. M. Hospedales. Deeper, broader and artier domain generalization. In *Proceedings of the IEEE international conference on computer vision*, pages 5542–5550, 2017.
- D. Li, Y. Yang, Y.-Z. Song, and T. Hospedales. Learning to generalize: Meta-learning for domain generalization. In *Proceedings of the AAAI Conference on Artificial Intelligence*, volume 32, 2018a.
- H. Li, S. J. Pan, S. Wang, and A. C. Kot. Domain generalization with adversarial feature learning. In *Proceedings of the IEEE Conference on Computer Vision and Pattern Recognition*, pages 5400–5409, 2018b.
- T. Li, A. Beirami, M. Sanjabi, and V. Smith. Tilted empirical risk minimization. *ICLR*, 2021.
- Y. Li, X. Tian, M. Gong, Y. Liu, T. Liu, K. Zhang, and D. Tao. Deep domain generalization via conditional invariant adversarial networks. In *Proceedings of the European Conference on Computer Vision (ECCV)*, pages 624–639, 2018c.
- Z. Li, L. Liu, C. Dong, and J. Shang. Overfitting or underfitting? understand robustness drop in adversarial training, 2020.
- A. Madry, A. Makelov, L. Schmidt, D. Tsipras, and A. Vladu. Towards deep learning models resistant to adversarial attacks. In *International Conference on Learning Representations*, 2018.
- H. Nam, H. Lee, J. Park, W. Yoon, and D. Yoo. Reducing domain gap by reducing style bias. In *Proceedings of the IEEE/CVF Conference on Computer Vision and Pattern Recognition*, pages 8690–8699, 2021.
- X. Peng, Q. Bai, X. Xia, Z. Huang, K. Saenko, and B. Wang. Moment matching for multi-source domain adaptation. In *Proceedings of the IEEE/CVF International Conference on Computer Vision*, pages 1406–1415, 2019.
- K. Qian, A. Beirami, Z. Lin, A. De, A. Geramifard, Z. Yu, and C. Sankar. Annotation inconsistency and entity bias in MultiWOZ. *The 22nd Annual Meeting of the Special Interest Group on Discourse and Dialogue (SIGDIAL)*, July 2021.
- A. Rastogi, X. Zang, S. Sunkara, R. Gupta, and P. Khaitan. Towards scalable multi-domain conversational agents: The schema-guided dialogue dataset, 2020.
- A. Ray, K. Sikka, A. Divakaran, S. Lee, and G. Burachas. Sunny and dark outside?! improving answer consistency in vqa through entailed question generation. In *EMNLP/IJCNLP*, 2019.

- M. T. Ribeiro, T. Wu, C. Guestrin, and S. Singh. Beyond accuracy: Behavioral testing of NLP models with CheckList. In *Proceedings of the 58th Annual Meeting of the Association for Computational Linguistics*, pages 4902–4912, Online, July 2020. Association for Computational Linguistics. doi: 10.18653/v1/2020.acl-main.442. URL <https://aclanthology.org/2020.acl-main.442>.
- S. Sagawa, P. W. Koh, T. B. Hashimoto, and P. Liang. Distributionally robust neural networks for group shifts: On the importance of regularization for worst-case generalization. *arXiv preprint arXiv:1911.08731*, 2019.
- M. Shah, X. Chen, M. Rohrbach, and D. Parikh. Cycle-consistency for robust visual question answering. In *2019 Conference on Computer Vision and Pattern Recognition (CVPR)*, 2019.
- B. Sun and K. Saenko. Deep coral: Correlation alignment for deep domain adaptation. In *European conference on computer vision*, pages 443–450. Springer, 2016.
- D. Tellez, G. Litjens, P. Bándi, W. Bulten, J.-M. Bokhorst, F. Ciompi, and J. van der Laak. Quantifying the effects of data augmentation and stain color normalization in convolutional neural networks for computational pathology. *Medical image analysis*, 58:101544, 2019.
- H. Venkateswara, J. Eusebio, S. Chakraborty, and S. Panchanathan. Deep hashing network for unsupervised domain adaptation. In *Proceedings of the IEEE conference on computer vision and pattern recognition*, pages 5018–5027, 2017.
- R. Volpi, H. Namkoong, O. Sener, J. Duchi, V. Murino, and S. Savarese. Generalizing to unseen domains via adversarial data augmentation. *arXiv preprint arXiv:1805.12018*, 2018.
- C.-S. Wu, A. Madotto, E. Hosseini-Asl, C. Xiong, R. Socher, and P. Fung. Transferable multi-domain state generator for task-oriented dialogue systems, 2019.
- M. Zaheer, S. Kottur, S. Ravanbakhsh, B. Póczos, R. R. Salakhutdinov, and A. J. Smola. Deep sets. In I. Guyon, U. V. Luxburg, S. Bengio, H. Wallach, R. Fergus, S. Vishwanathan, and R. Garnett, editors, *Advances in Neural Information Processing Systems*, 2017.
- X. Zang, A. Rastogi, S. Sunkara, R. Gupta, J. Zhang, and J. Chen. Multiwoz 2.2 : A dialogue dataset with additional annotation corrections and state tracking baselines, 2020.
- H. Zhang, M. Cisse, Y. N. Dauphin, and D. Lopez-Paz. mixup: Beyond empirical risk minimization. *arXiv preprint arXiv:1710.09412*, 2017.
- H. Zhang, Y. Yu, J. Jiao, E. Xing, L. E. Ghaoui, and M. Jordan. Theoretically principled trade-off between robustness and accuracy. In *International Conference on Machine Learning*, 2019.
- H. Zheng, Z. Zhang, J. Gu, H. Lee, and A. Prakash. Efficient adversarial training with transferable adversarial examples. In *Proceedings of the IEEE Conference on Computer Vision and Pattern Recognition (CVPR)*, 2020.
- K. Zhou, Y. Yang, T. Hospedales, and T. Xiang. Deep domain-adversarial image generation for domain generalisation. In *Proceedings of the AAAI Conference on Artificial Intelligence*, volume 34, pages 13025–13032, 2020.

A Proofs

Proof of Proposition 1. First let us present the DA-ERM solution:

$$f_{\text{DA-ERM}}(w) = \mathbb{E} [(w_1x + w_2y - y)^2 + (w_1x + w_2(ay + n) - y)^2] \quad (1)$$

$$\begin{aligned} &= \mathbb{E} [w_1^2x^2 + (w_2 - 1)^2y^2 + 2w_1(w_2 - 1)xy] \\ &\quad + \mathbb{E} [w_1^2x^2 + (w_2a - 1)^2y^2 + w_2^2n^2] \\ &\quad + \mathbb{E} [2w_1(w_2a - 1)xy + 2w_1w_2xn + 2w_2(w_2a - 1)yn] \end{aligned} \quad (2)$$

$$\begin{aligned} &= w_1^2\sigma_x^2 + (w_2 - 1)^2(\sigma_x^2 + \sigma_\varepsilon^2) + 2w_1(w_2 - 1)\sigma_x^2 \\ &\quad + w_1^2\sigma_x^2 + (w_2a - 1)^2(\sigma_x^2 + \sigma_\varepsilon^2) + w_2^2\sigma_n^2 \\ &\quad + 2w_1(w_2a - 1)\sigma_x^2 \end{aligned} \quad (3)$$

$$\begin{aligned} &= (w_1 + w_2 - 1)^2\sigma_x^2 + (w_2 - 1)^2\sigma_\varepsilon^2 \\ &\quad + (w_1 + w_2a - 1)^2\sigma_x^2 + (w_2a - 1)^2\sigma_\varepsilon^2 + w_2^2\sigma_n^2. \end{aligned} \quad (4)$$

Hence, the solution of $w_{\text{DA-ERM}}^* = \arg \min_w f_{\text{DA-ERM}}(w)$ is given by

$$\begin{aligned} &2w_1^* + (1 + a)w_2^* - 2 = 0, \\ &(w_1^* + w_2^* - 1)\sigma_x^2 + (w_2^* - 1)\sigma_\varepsilon^2 + a(w_1^* + w_2^*a - 1)\sigma_x^2 + a(w_2^*a - 1)\sigma_\varepsilon^2 + w_2^*\sigma_n^2 = 0. \end{aligned} \quad (5)$$

Subsequently,

$$w_{\text{DA-ERM}}^* = \begin{pmatrix} \frac{a^2(\sigma_x^2 + \sigma_\varepsilon^2) - 2a(\sigma_x^2 + \sigma_\varepsilon^2) + \sigma_x^2 + \sigma_\varepsilon^2 + 2\sigma_n^2}{a^2(\sigma_x^2 + 2\sigma_\varepsilon^2) - 2a\sigma_x^2 + \sigma_x + 2(\sigma_\varepsilon^2 + \sigma_n^2)} \\ \frac{2(a+1)\sigma_\varepsilon^2}{a^2(\sigma_x^2 + 2\sigma_\varepsilon^2) - 2a\sigma_x^2 + \sigma_x + 2(\sigma_\varepsilon^2 + \sigma_n^2)} \end{pmatrix}. \quad (6)$$

$$\begin{aligned} w_{\text{DAIR}}^* &= \arg \min_w f_{\text{DAIR}}(w) \\ &= \arg \min_w \mathbb{E} [(w_1x + w_2y - y)^2 + (w_1x + w_2(ay + n) - y)^2] \\ &\quad + [\lambda(|w_1x + w_2y - y| - |w_1x + w_2(ay + n) - y|)^2]. \end{aligned}$$

When $\lambda \rightarrow \infty$, we have $w_{\text{DAIR},2}^* = 0$ and hence:

$$w_{\text{DAIR}}^* = \begin{pmatrix} 1 \\ 0 \end{pmatrix}.$$

We then evaluate the testing loss assuming the spurious feature is absent, i.e., $\mathbf{x}_{\text{test}} = (x, s = 0)$.

$$\begin{aligned} \ell_{\text{DAIR}}(\mathbf{x}_{\text{test}}; w_{\text{DAIR}}^*) &= \mathbb{E} [(w_{\text{DAIR}}^* \top \mathbf{x}_{\text{test}} - y)^2] \\ &= \mathbb{E} [(x - (x + \varepsilon))^2] \\ &= \sigma_\varepsilon^2. \end{aligned}$$

$$\begin{aligned} \ell_{\text{DA-ERM}}(\mathbf{x}_{\text{test}}; w_{\text{DA-ERM}}^*) &= \mathbb{E} [(w_{\text{DA-ERM}}^* \top \mathbf{x}_{\text{test}} - y)^2] \\ &= \mathbb{E} \left[\left(\frac{a^2(\sigma_x^2 + \sigma_\varepsilon^2) - 2a(\sigma_x^2 + \sigma_\varepsilon^2) + \sigma_x^2 + \sigma_\varepsilon^2 + 2\sigma_n^2}{a^2(\sigma_x^2 + 2\sigma_\varepsilon^2) - 2a\sigma_x^2 + \sigma_x + 2(\sigma_\varepsilon^2 + \sigma_n^2)} x - (x + \varepsilon) \right)^2 \right] \\ &= \sigma_\varepsilon^2 + \frac{(a+1)^4\sigma_\varepsilon^4\sigma_x^2}{(a^2(\sigma_x^2 + 2\sigma_\varepsilon^2) - 2a\sigma_x^2 + \sigma_x + 2(\sigma_\varepsilon^2 + \sigma_n^2))^2} \\ &\geq \ell_{\text{DAIR}}. \end{aligned}$$

Proof of Lemma 1. We proceed as follows:

$$r_{\ell_1}(z, \tilde{z}; \theta) - r_{\text{sq}}(z, \tilde{z}; \theta) = 2\sqrt{\min\{\ell(z; \theta), \ell(\tilde{z}; \theta)\}} \left| \sqrt{\ell(\tilde{z}; \theta)} - \sqrt{\ell(z; \theta)} \right|,$$

We break it into two cases: if $\ell(\tilde{z}; \theta) > \ell(z; \theta)$:

$$\begin{aligned} r_{\ell_1}(z, \tilde{z}; \theta) - r_{\text{sq}}(z, \tilde{z}; \theta) &= \ell(\tilde{z}; \theta) - \ell(z; \theta) - (\sqrt{\ell(\tilde{z}; \theta)} - \sqrt{\ell(z; \theta)})^2 \\ &= \ell(\tilde{z}; \theta) - \ell(z; \theta) - \ell(\tilde{z}; \theta) - \ell(z; \theta) + 2\sqrt{\ell(\tilde{z}; \theta)}\sqrt{\ell(z; \theta)} \\ &= -2\ell(z; \theta) + 2\sqrt{\ell(\tilde{z}; \theta)}\sqrt{\ell(z; \theta)} \\ &= 2\sqrt{\ell(z; \theta)}(\sqrt{\ell(\tilde{z}; \theta)} - \sqrt{\ell(z; \theta)}). \end{aligned}$$

If $\ell(\tilde{z}; \theta) \leq \ell(z; \theta)$:

$$\begin{aligned} r_{\ell_1}(z, \tilde{z}; \theta) - r_{\text{sq}}(z, \tilde{z}; \theta) &= \ell(z; \theta) - \ell(\tilde{z}; \theta) - (\sqrt{\ell(\tilde{z}; \theta)} - \sqrt{\ell(z; \theta)})^2 \\ &= \ell(z; \theta) - \ell(\tilde{z}; \theta) - \ell(\tilde{z}; \theta) - \ell(z; \theta) + 2\sqrt{\ell(\tilde{z}; \theta)}\sqrt{\ell(z; \theta)} \\ &= -2\ell(\tilde{z}; \theta) + 2\sqrt{\ell(\tilde{z}; \theta)}\sqrt{\ell(z; \theta)} \\ &= 2\sqrt{\ell(\tilde{z}; \theta)}(\sqrt{\ell(z; \theta)} - \sqrt{\ell(\tilde{z}; \theta)}). \end{aligned}$$

If we combine the two cases, we have:

$$r_{\ell_1}(z, \tilde{z}; \theta) - r_{\text{sq}}(z, \tilde{z}; \theta) = 2\sqrt{\min\{\ell(z; \theta), \ell(\tilde{z}; \theta)\}} \left| \sqrt{\ell(\tilde{z}; \theta)} - \sqrt{\ell(z; \theta)} \right|.$$

B Model Architecture and Training Parameters for MNIST Experiments

Layer Type	Shape
Convolution + ReLU	$4 \times 4 \times 6$
Max Pooling	2×2
Convolution + ReLU	$4 \times 4 \times 16$
Max Pooling	2×2
Convolution + ReLU	$4 \times 4 \times 96$
Fully Connected + ReLU	64
Fully Connected	C

Table 5: Model Architecture, $C = 1$ for Colored MNIST and $C = 10$ for Rotated MNIST

Parameter		
Learning Rate	0.005	0.0005
Epochs	20	20
Batch-size	64	

Table 6: Training parameter

C Setup and Additional Results for VQA

We modify the official code released by Agarwal et al. [2020] to suit our formulation. All the methods are trained for 40 epochs with a learning rate of 0.001 and a batch size of 96.

Table 7 indicates a tradeoff between the accuracy on the VQA v2 ‘val’ set and the consistency metrics. As the λ value increases, the consistency between the predictions increases, while the accuracy on original examples decreases. For instance, A λ value of 10 strongly boosts consistency thus lowering the ‘Predictions flipped’ percentage to only 7.9% but sacrifices the predictive power causing the accuracy to drop to 51.3 %

λ	VQA v2 val (%)	Predictions flipped (%)	pos \rightarrow neg (%)	neg \rightarrow pos (%)	neg \rightarrow neg (%)
0.37	58.52	11.92	4.48	5.28	2.17
0.72	58.21	11.28	4.13	5.08	2.07
1.39	57.54	10.37	3.80	4.65	1.91
2.68	56.24	9.68	3.56	4.39	1.73
5.18	54.19	8.75	3.40	3.66	1.69
10	51.32	7.94	3.01	3.40	1.53

Table 7: Accuracy-Consistency Tradeoff on VQA v2 val and IV-VQA test set controlled by λ

Scheme	z	Color $y = 0$
C1	with $p = 0.8, z = y$	Red
	with $p = 0.2, z = 1 - y$	Green
C2	with $p = 0.9, z = y$	Red
	with $p = 0.1, z = 1 - y$	Green
C3	with $p = 0.1, z = y$	Red
	with $p = 0.9, z = 1 - y$	Green
C4	$z = 2$	Random

Table 8: Color schemes in Colored MNIST. Random color means that the value of each channel of the image is uniformly random chosen from 0 to 255.

D Colored MNIST & Rotated MNIST Setup

We apply the proposed loss function (DAIR) on the following two datasets: Colored MNIST and Rotated MNIST. We compare the performance of DAIR with plain data augmentation, and invariant risk minimization (IRM) as a strong baseline. One crucial difference between our work and IRM is the motivation. IRM is designed to take two examples from two different environments and learn representations that are invariant to the environment, e.g., in cases where we are aggregating multiple datasets. On the other hand, we are interested in promoting invariance when we have a single dataset. As such, we artificially generate the second environment in IRM using data augmentation. For a given example z , we design an augmenter $A(\cdot)$ and use it to generate additional samples that adhere to the invariance we have in mind. Hence, IRM will be applied in the same way that examples from different environments are augmenting pairs.

Our Colored MNIST is an extension of the original Colored MNIST Arjovsky et al. [2019]. The label is a noisy function of both digit and color. The digit has a correlation of 0.75 with the label and a certain correlation with the label depending on the color scheme. Besides the two colors in the original dataset, we introduce fully random colored scheme to the dataset, which is the best augmenter one can think of. The three color schemes are detailed in Table 8.

Our Rotated MNIST is a variant of the original Rotated MNIST [Ghifary et al., 2015]. The original dataset contains images of digits rotated d degrees, where $d \in \mathcal{D} \triangleq \{0, 15, 30, 45, 60, 75\}$. Similarly, we introduce the random degree scheme here to serve as the best possible augmenter. To further exploit the potential of the proposed algorithm, we make this dataset more difficult by introducing more challenging degree scheme; The rotation schemes are summarized in Table 9.

Note all the augmented images are generated on the fly. Examples of images from some transformation schemes are shown in Figures 8 to 13.

Setup	Train	Aug	Test	λ
Strong Aug.	R1	R5	R2	1
Weak Aug.	R4	R6	R3	10

Table 11: Training procedure of Rotated MNIST

Scheme	Rotation
R1	0°
R2	90°
R3	0°, 180°
R4	90°, 270°
R5	[0°, 360°]
R6	[22.5°, 67.5°], [202.5°, 247.5°]

Table 9: Rotation schemes in Rotated MNIST. $[a, b]$ means that degrees are uniformly random chosen between a and b .

Setup Name	Train	Aug	Test	λ
Adv. Aug.	C1	C2	C3	1000
Rnd. Aug.	C1	C4	C3	100

Table 10: Training procedure of Colored MNIST.

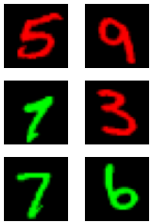


Figure 8: C2

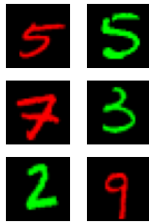


Figure 9: C3



Figure 10: C4



Figure 11: R4



Figure 12: R5



Figure 13: R6

Setup: We train a model consisted of three convolutional layers and two fully connected layers with 20,000 examples. For each dataset we are defining several different schemes on how the dataset could be modified: Table 8 (Colored MNIST) and Table 9 (Rotated MNIST). Then, we define several *setups*. Each setup is consisted of one original dataset, one augmentation dataset, and one test dataset, each of which is selected among the defined schemes. These setups are provided in Table 10 (Colored MNIST) and Table 11 (Rotated MNIST). For each setup, we train the model with the following four algorithms and compare their performances: ERM, DA-ERM, DAIR and Invariant Risk Minimization (IRM). Each experiment is repeated for 10 times; the mean and the standard derivation are reported. The value of λ are chosen base on the validation results. Detailed architectures and training parameters can be found in Appendix B.

D.1 Colored MNIST

We conduct two sets of experiments for this dataset: Adversarial Augmentation Setup (Table 10) follows the exact same color schemes from the original Colored MNIST Arjovsky et al. [2019]. For Random Augmentation Setup, we train the model with the strongest possible augmenter: uniformly random color. The entire procedure is summarized in Table 10.

D.2 Rotated MNIST

We start with the strongest augmenter case. One may notice that there is a chance that the augmented images bear the same rotation degrees as the testing set. To make the task more difficult, we will use R6 as the augmented test to test how the trained model generalize to entirely unseen domain. The training procedure is summarized in Table 11.